

# A Pulse-Shape Binary Multiplex Modulation

Pavel Loskot, *Senior Member, IEEE*

## Abstract

The root raised-cosine pulse commonly used in linear digital modulations yields exactly two intersymbol interference components from the preceding and the subsequent data symbols, provided that the roll-off factor is 100% and the modulation packing factor is set to 50%. This can be exploited to symmetrically multiplex two data streams of transmitted symbols. Hence, the proposed scheme is referred to as pulse-shape binary multiplex modulation. The demodulation of the two multiplexed data streams at the receiver can be aided by making the streams mutually orthogonal. It can be achieved by superposition modulation with symbol-by-symbol interference cancellation, proper design of transmission sequences interleaving pilot and data symbols in order to also enable channel estimation, and using orthogonal spreading sequences. The presented numerical results indicate that the proposed modulation scheme can outperform Nyquist signaling in terms of transmission reliability or the time required for transmitting the whole sequence of data symbols. For instance, differentially encoded modulation symbols can be transmitted twice as fast by the proposed modulation scheme with a 3 dB penalty in signal-to-noise ratio over additive white Gaussian noise channels.

## Index Terms

Intersymbol-interference; linear modulation; Nyquist signaling; partial response signaling; root raised cosine pulse; sequence multiplexing.

## I. INTRODUCTION

The spectrum scarcity necessities the use of spectrally efficient modulations. The Nyquist signaling is a well established and robust technique for constructing linear digital modulations which are employed in a vast majority of today's communication systems. These modulation schemes are often combined with channel encoding to improve the transmission reliability and even approach the channel capacity. An alternative strategy is to assume modulations having a controlled level of intersymbol interference (ISI), which can increase the rate of information transmission as well as act as a form of information encoding for improving the transmission

The author is with ZJU-UIUC Institute, Haining, China (e-mail: pavelloskot@intl.zju.edu.cn).

This work was supported by a research grant from Zhejiang University.

reliability [1], albeit at the cost of increased detection complexity at the receiver. Such so-called faster-than-Nyquist (FTN) schemes are linear modulations that can be used over band-limited channels [2].

The renewed interest in FTN signaling schemes goes back to the early 2000's [3]. However, a closely related idea of partial response linear modulations with controlled ISI appeared much earlier [4]. The achievable spectral efficiency of coded and uncoded FTN schemes is evaluated in [2], [5], and [6]. The observation that up to 25% increase in the transmission rate is possible without deteriorating the error performance is known as the Mazo limit [3], [2], [7], [6]. The energy and complexity costs of FTN signaling are reviewed in [2].

The FTN schemes can be implemented both in time and in frequency domains [2], [8]. An orthogonal FTN scheme based on OFDM was designed in [9]. Alternatively, Nyquist signaling with dual root raised-cosine (RRC) pulses akin to duobinary modulation has been investigated in [10]. This scheme was further refined for the RRC pulses with zero roll-off in [11]. The link between duobinary modulation and FTN signaling has been pointed out in [1].

An important issue is how to efficiently perform the detection of transmitted symbols at the receiver. Unlike the ISI due to multipath propagation, the ISI created by FTN signaling also correlates samples of additive noise. The optimum detection necessitates the use of whitening matched filter (WMF) prior to symbol decisions. The ISI at the detector input can be equivalently represented as an auxiliary channel [5], [6]. The output signal of such channel has a trellis-like structure, which can be optimally equalized by the Viterbi, BCJR and other such algorithms with varying complexity [2], [7], [6]. These decoding methods can approach the performance of zero-ISI (Nyquist) modulations over additive white Gaussian noise (AWGN) channels [2]. The symbol-by-symbol detector for FTN signals was devised in [6] and [12]. The detection of FTN signals with oversampling and one-bit quantization was developed in [5]. A low complexity linear equalization for FTN signaling was designed in [13]. The joint channel estimation and decoding of FTN signals was studied in [14] and in [15].

Nearly all investigations of FTN signaling schemes in the literature assume the RRC modulation pulse. The RRC pulse is parameterized by a time period,  $T_p$ , and a roll-off factor,  $\alpha$ . Linear modulations combine the RRC pulses weighted by data symbols, which are then transmitted once every symbol period,  $T_s$ . The packing factor defines the relationship between  $T_p$  and  $T_s$ , i.e.,  $\tau = 1 - T_s/T_p$ . The design and analysis of FTN signaling in the literature usually assumes arbitrary values of  $0 \leq \alpha \leq 1$  and  $0 \leq \tau < 1$ . The search for good values of  $\alpha$  and  $\tau$  over an

entire  $\alpha - \tau$  plane to allow symbol-by-symbol decisions was carried out in [12]. However and importantly, the case of 100% bandwidth roll-off is rarely explicitly considered in the literature [6]. The authors in [5] noticed that, for  $\alpha = 1$  and an arbitrary value of  $\tau$ , the ISI is approximately limited to the two previous and the two subsequent symbol samples.

In this paper, we show that the RRC pulse with 100% roll-off and 50% packing has a well-defined ISI, which is exactly and symmetrically constrained to one previous and one subsequent symbol. Such a unique property of the RRC pulse appears to remain unnoticed in the literature. Interestingly, reference [1] states that ISI with only two components can be obtained with 100% roll-off and 50% packing assuming prolate spheroidal wave pulses, but not RRC pulses. Although such a modulation scheme can be assumed to be a special case of FTN signaling, it is argued that RRC pulses having 100% roll-off and 50% packing offers symmetric multiplexing of the two transmitted data streams. For this reason, such a partial response signaling is referred to in this paper as a pulse-shape binary multiplexing (PSBM) modulation. The main task then is how to separate the two multiplexed data streams at the receiver with acceptable reliability and complexity. As with other partial response signalings, the modulation constellation and the dependency between transmitted symbols must be carefully selected in order to trade-off the performance and the decoding complexity. We design several transmission sequences interleaving pilot and data symbols, discuss superposition modulation with symbol-by-symbol sequential interference cancellation (SIC), and also consider orthogonal spreading sequences to aid separation of the data streams at the receiver. In addition, the performance of multiplexed differentially encoded phase-shift keying (PSK) modulation symbols is evaluated numerically. The numerical results identify several cases when the proposed PSBM modulation outperforms the Nyquist signaling in terms of either transmission reliability or the time required to transmit a given number of data symbols.

The rest of this paper is organized as follows. Linear modulation schemes that are related to the proposed pulse-shape multiplexing signaling are outlined in Section II. System model and the received signal structure are described in Section III. The proposed pulse-shape multiplexing modulation is defined in Section IV including the design of transmitted symbol sequences. Numerical results are presented in Section V. Section VI concludes the paper.

We adopt the following notations:  $E[\cdot]$  is expectation,  $\otimes$  is convolution,  $|\cdot|$  is absolute value,  $(\cdot)^*$  is complex conjugate,  $\text{Re}\{\cdot\}$  and  $\text{Im}\{\cdot\}$ , respectively, denote the real and imaginary part of a complex number,  $\text{Card}\{\cdot\}$  is cardinality of a set,  $(\cdot)^T$  is matrix transpose,  $(\cdot)^{-1}$  is matrix

inverse, and  $\|\cdot\|$  is the Euclidean norm of a matrix or vector.

## II. RELATED LINEAR MODULATION SCHEMES

A linearly modulation signal is constructed as,

$$x(t) = \sum_k s_k p(t - kT_s) \quad (1)$$

where  $s_k$  are  $M$ -ary modulation symbols transmitted every symbol period,  $T_s$ , and  $p(t)$  denotes a deterministic pulse-shape, which is also known at the receiver. The stationary sequence of transmitted symbols,  $s_k$ , has zero-mean, and the variance,  $E[|s_k|^2] = E_s$ . The symbols are usually obtained as output of a finite-state modulator, i.e.,

$$s_k = s(q_k, c_k) \quad (2)$$

where the states,  $q_k$ , represent modulation memory, and the data symbols,  $c_k$ , each carry,  $\log_2 M$ , bits of input information. In this paper,  $p(t)$  is assumed to be the unit-energy RRC pulse, [4]

$$p(t) = \frac{\text{rrc}_\alpha(t/T_s)}{\sqrt{T_s}} \quad (3)$$

where

$$\text{rrc}_\alpha(t) = \frac{1}{1 - 16\alpha^2 t^2} \left( \frac{\sin((1 - \alpha)\pi t)}{\pi t} + \frac{4\alpha \cos((1 + \alpha)\pi t)}{\pi} \right). \quad (4)$$

The roll-off factor,  $0 \leq \alpha \leq 1$ , however, it is possible to also consider pulse shapes having a roll-off greater than 100%.

Since the sequence of symbols,  $s_k$ , is stationary, the auto-correlation,  $R_s(i - j) = E[s_i s_j^*]$ . The corresponding power-spectrum density (PSD) of signal (1) is computed as, [4]

$$S_x(f) = \frac{1}{T_s} |P(f)|^2 \sum_k R_s(k) e^{j2\pi f k T_s} \quad (5)$$

where  $P(f)$  denotes the Fourier transform of  $p(t)$ .

Correlative coding assumes the discrete modulator (2) to be a finite impulse response (FIR) filter, i.e.,

$$s_k = \sum_{i=0}^{K-1} v_i c_{k-i}. \quad (6)$$

The filter weights,  $v_i$ , are normalized, so that,  $\sum_i |v_i|^2 = 1$ . More importantly, with a change in indices, modulated signal (1) with symbols (6) can be rewritten as,

$$\begin{aligned} x(t) &= \sum_k \sum_{i=0}^{K-1} v_i c_{k-i} p(t - kT_s) \\ &= \sum_k c_k \sum_{i=0}^{K-1} v_i p(t - (k+i)T_s) = \sum_k c_k \tilde{p}(t - kT_s) \end{aligned} \quad (7)$$

where the compound pulse,  $\tilde{p}(t) = \sum_{i=0}^{K-1} v_i p(t - iT_s)$ .

Duobinary modulation is a special case of correlative coding, such that the FIR filter has only two non-zero weights,  $v_0 = v_1 = 1/\sqrt{2}$ , the modulation symbols are binary, i.e.,  $c_k \in \{-\sqrt{E_s}, +\sqrt{E_s}\}$ , and the RRC pulse has the smallest possible roll-off,  $\alpha = 0$ . Modified duobinary modulation assumes instead the weights,  $v_0 = 1/\sqrt{2}$ ,  $v_1 = 0$ , and  $v_2 = -1/\sqrt{2}$ .

The following modulations assume the RRC pulse-shape with an arbitrary roll-off value. Differential PSK constructs the transmitted symbols as,

$$s_k = c_k s_{k-1} \quad (8)$$

where the data symbols,  $c_k \in \{\sqrt{E_s} e^{j2\pi(i-1)/M}\}$ ,  $i = 1, 2, \dots, M$ . Generalized shift-keying extends the modulation alphabet of amplitude or phase shift-keying modulations with a zero symbol [16]. Offset-quadrature ( $M = 4$ ) PSK delays the imaginary part of the modulated signal by half a symbol period, i.e.,

$$x(t) = \sum_k \text{Re}\{c_k\} p(t - kT_s) + j \text{Im}\{c_k\} p(t - kT_s - T_s/2). \quad (9)$$

Finally, FTN signaling is a linear modulation described by eq. (1). More importantly, the RRC pulse-shape in (3) can now be scaled by,  $T_p = T_s/(1 - \tau)$ , instead of  $T_s$ , where  $0 \leq \tau < 1$  is so-called the packing factor, i.e.,

$$x(t) = \sum_k s_k p(t - k(1 - \tau)T_p) = \sum_k s_k p(t - kT_s) \quad (10)$$

so that  $T_p$  is a design parameter of the pulse,  $p(t)$ , whereas,  $T_s = (1 - \tau)T_p$ , denotes the symbol period. Thus,  $\tau = 0$  packing corresponds to a conventional Nyquist signaling, whereas  $\tau = 1$  packing would completely overlap the transmitted symbols. More importantly, the PSD of (10) is still given by eq. (5), and it is otherwise completely independent of the packing factor,  $\tau$ .

### III. RECEIVED SIGNAL

The standard wireless channel model with  $L$  propagation paths is an FIR filter with the impulse response,

$$\tilde{h}(t) = \sum_{l=1}^L h_l(t) \delta(t - \tau_l). \quad (11)$$

The signal delays,  $\tau_l$ , are assumed to be constant. The path attenuations,  $h_l(t)$ , are zero-mean circularly symmetric Gaussian processes. These processes are stationary, and generally mutually correlated. They have a defined auto-correlation,  $R_h(\Delta t)$ , which determines the coherence bandwidth.

For narrow-band signals, the number of paths,  $L$ , is small. For  $L = 1$ , the channel model (11) becomes frequency non-selective. In low-mobility scenarios, the channel attenuations,  $h_l(t)$ , are often assumed to be constant over blocks of transmitted symbols, and independent between the successive blocks, which is often referred to as a block fading model.

The received signal corresponding to multi-path propagation model (11) is written as,

$$\begin{aligned} y(t) &= \tilde{h}(t) \otimes x(t) + w(t) \\ &= \sum_{l=1}^L h_l(t) x(t - \tau_l) + w(t) \end{aligned} \quad (12)$$

where  $w(t)$  is a zero-mean stationary circularly symmetric AWGN with the variance,  $\sigma_w^2 = \text{E}[|w(t)|^2]$ .

The received signal is filtered through a filter matched to the transmitted pulse,  $p(t)$ , and synchronously sampled at a rate,  $1/T_s$ . In particular, assuming RRC pulses, the matched filter,  $p^*(-t) = p(t)$ , and provided that the channel attenuations are constant over blocks of transmitted

symbols, the received samples are modeled as,

$$\begin{aligned}
r_n &= y(t) \otimes p^*(-t) \Big|_{t=nT_s+\tau_0} \\
&= \sum_{l=1}^L h_l x(t - \tau_l) \otimes p(t) \Big|_{t=nT_s+\tau_0} + w(t) \otimes p(t) \Big|_{t=nT_s+\tau_0} \\
&= \sum_{l=1}^L h_l \sum_k s_k \int_{-\infty}^{\infty} p(\zeta + (n-k)T_s - \tau_l) p(\zeta - \tau_0) d\zeta \\
&\quad + \int_{-\infty}^{\infty} w(\zeta + nT_s) p(\zeta - \tau_0) d\zeta \\
&= \sum_k s_k \sum_{l=1}^L h_l p_{n-k,l} + w_n = \sum_k s_k \tilde{p}_{n-k} + w_n \\
&= s_k \tilde{p}_0 + \underbrace{\sum_{\substack{k \\ n \neq k}} s_k \tilde{p}_{n-k}}_{\text{ISI}} + w_n.
\end{aligned} \tag{13}$$

The timing offset,  $\tau_0$ , at the receiver can be optimized to minimize the ISI term (in some sense) in (13) defined as,

$$\tilde{p}_{n-k} = \sum_{l=1}^L h_l \int_{-\infty}^{\infty} p(\zeta + (n-k)T_s - \tau_l) p(\zeta - \tau_0) d\zeta, \quad n \neq k. \tag{14}$$

Thus, the ISI arises when the orthogonality between the transmitter and the receiver pulses is violated, for example, due to multi-path propagation, time-synchronization errors between transmitter and receiver, and also due to symbol-period compression in FTN signaling schemes [4].

An interesting question is how much ISI is produced for different combinations of parameters  $\alpha$  and  $\tau$  in FTN signaling schemes using RRC pulses. Hence, define the function,

$$\text{ISI}(\mu) = \text{Card}\{|\tilde{p}_k| > \mu, \quad k \neq 0\} \tag{15}$$

to be the number of ISI components that are greater than a given threshold,  $\mu$ . Note that,  $\text{ISI}(\mu) \in \{0, 2, 4, \dots\}$ , due to even symmetry of the RRC pulses. Assuming different thresholds,  $\mu$ , the roll-off,  $0 \leq \alpha \leq 2$ , and the RRC pulses truncated to  $(-4T_s, +4T_s)$ , the values  $\text{ISI}(\mu) = 0$  (red points) and  $\text{ISI}(\mu) = 2$  (blue points) in the  $\alpha - \tau$  plane are shown in Fig. 1. The empty (white) spaces in Fig. 1 indicate the values,  $\text{ISI}(\mu) > 2$ . It can be observed that by decreasing the threshold,  $\mu$ , several cases of interest for designing FTN signaling schemes start to emerge. In particular, exactly two ISI components can be obtained for these parameters:  $\alpha = 1.0$  and  $\tau = 0.5$ ,  $\alpha = 1.07$  and  $\tau \in (0.70, 0.71)$ , and  $\alpha \in (1.65, 1.85)$  and  $\tau \in (0.47, 0.50)$ .

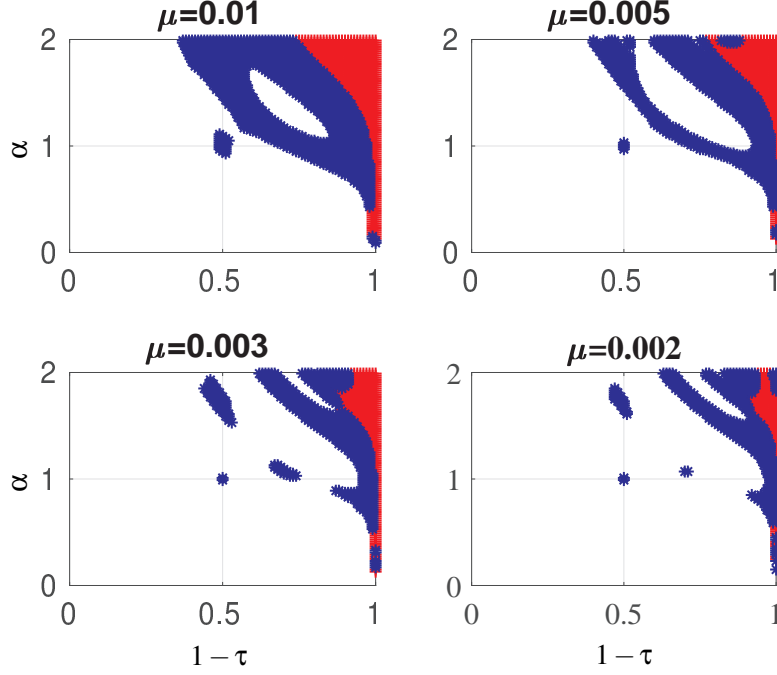


Fig. 1. The  $\text{ISI}(\mu) = 0$  components (red points) and  $\text{ISI}(\mu) = 2$  components (blue points) for four different thresholds,  $\mu$ .

#### IV. PULSE-SHAPE BINARY MULTIPLEX MODULATION

As indicated in Fig. 1, the RRC pulse with 100% roll-off and 50% packing has well-defined and finite ISI components. In particular, the RRC pulse (4) for  $\alpha = 1$  becomes,

$$\text{rrc}_1(t) = \frac{4 \cos(2\pi t)}{\pi(1 - 16t^2)}. \quad (16)$$

This pulse has the following ISI components in an AWGN channel without multi-path. Such a fundamental property appears to remain unnoticed in the literature.

*Lemma 1:* Let  $n$  be a non-negative integer. The ISI integral involving the RRC pulse,  $\text{rrc}_1(t)$ , with 100% roll-off has the exact solution,

$$\begin{aligned} & \int_{-\infty}^{\infty} \text{rrc}_1(t) \times \text{rrc}_1(t - n/4) dt \\ &= \begin{cases} 8/(3\pi) & n = 1 \\ \frac{8}{\pi(n-2)n(n+2)} & n - \text{odd}, n > 1 \\ 1 & n = 0 \\ 1/2 & n = 2 \\ 0 & n - \text{even}, n > 2. \end{cases} \end{aligned} \quad (17)$$



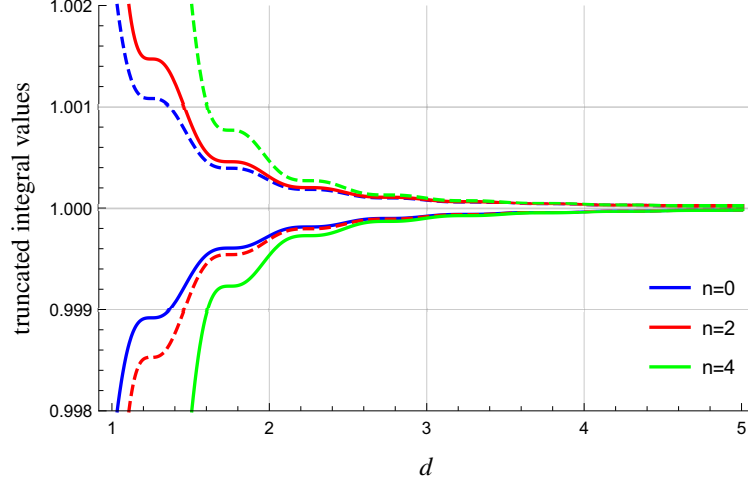


Fig. 2. Numerically computed integral (17) truncated to interval,  $(-d, +d)$ , as a function of  $d$  (solid lines). The exact values for an infinite interval are shifted to be all equal to unity in order to enable comparison. The dashed lines are mirrored solid lines about the unit value.

Lemma 1 can be proved by solving the integral for the first few values of  $n$  (for example, using Mathematica software), and then using induction.

However, the result (17) is exact only when the integration is performed over an infinite interval. In practice, the pulse shapes must be truncated to a finite interval. The numerically computed values of integral (17) when the interval of integration is truncated to  $(-d, +d)$  are shown in Fig. 2. It can be observed that the RRC pulse shape,  $\text{rrc}_1(t)$ , should not be truncated to the intervals shorter than,  $(-4, +4)$ , in order to achieve the RRC property given in Lemma 1 with at least 99.9% accuracy.

*Definition 2:* The modulated signal of pulse-shape binary multiplex modulation is written as,

$$x(t) = \sum_k s_k \frac{\text{rrc}_1\left(\frac{t-kT_s}{2T_s}\right)}{\sqrt{2T_s}}. \quad (18)$$

The synchronously sampled matched filter output of modulated signal (18) received in AWGN,  $w(t)$ , is,

$$\begin{aligned} r_n &= (x(t) + w(t)) \otimes \frac{\text{rrc}_1\left(\frac{t}{2T_s}\right)}{\sqrt{2T_s}} \Big|_{t=nT_s} \\ &= \sum_k s_k \int_{-\infty}^{\infty} \text{rrc}_1(\zeta + (n-k)/2) \text{rrc}_1(\zeta) d\zeta + w_n \\ &= \left( \frac{1}{2} s_{n-1} + s_n + \frac{1}{2} s_{n+1} \right) + w_n. \end{aligned} \quad (19)$$

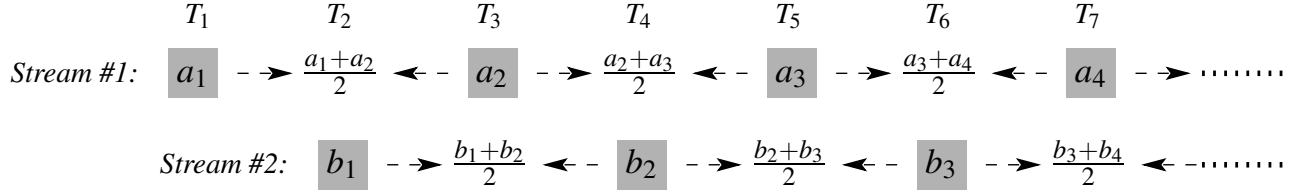


Fig. 3. A visualization of pulse-shape multiplex modulated signal.

The noise samples,  $w_n$ , in (19) are zero-mean, have the variance,  $E[|w_n|^2] = E[|w(t)|^2] = \sigma_w^2$ , and their stationary auto-correlation is,

$$R_w(n - m) = E[w_n w_m^*] = \begin{cases} \sigma_w^2 & n = m \\ \sigma_w^2/2 & |n - m| = 1 \\ 0 & |n - m| > 1. \end{cases} \quad (20)$$

Such noise samples can be equivalently modeled by a simple FIR filter,

$$w_n = \frac{u_n + u_{n-1}}{\sqrt{2}} \quad (21)$$

where  $u_n$  are the samples of a zero-mean, circularly symmetric Gaussian process having the variance,  $E[|u_n|^2] = \sigma_w^2$ . In addition, it is straightforward to show that the variance of the sum of  $N$  noise samples having the correlations (20) is,

$$\text{var} \left[ \sum_{n=1}^N w_n \right] = (2N - 1) \sigma_w^2 \quad (22)$$

which is greater than the variance,  $N\sigma_w^2$ , of the sum of  $N$  uncorrelated samples.

The modulated signal (18) in Definition 2 can be visualized as shown in Fig. 3. In particular, the transmitted data symbols can be viewed as consisting of two multiplexed streams of data symbols,  $a_k$ , and,  $b_k$ , which are each transmitted with a period  $2T_s$ , but mutually shifted by  $T_s$ .

The corresponding received symbol samples after the matched filtering are,

$$r_n = \begin{cases} a_n + \frac{b_{n-1} + b_n}{2} + w_n & n - \text{odd} \\ b_n + \frac{a_n + a_{n+1}}{2} + w_n & n - \text{even}. \end{cases} \quad (23)$$

Using (5), the PSD of modulated signal (18) is computed as,

$$S_x(f) = 2|\text{RRC}_1(2T_s f)|^2 \sum_k E[s_0 s_k^*] e^{j2\pi f k T_s} \quad (24)$$

where the Fourier transform of the pulse,  $\text{rrc}_1(t)$ , is,

$$\text{RRC}_1(f) = \begin{cases} \cos(\pi f/2) & |f| \leq 1 \\ 0 & \text{otherwise.} \end{cases} \quad (25)$$

### A. Transmitted Sequence Design

The optimum detection of transmitted symbols in the presence of ISI must consider complete sequences of received samples. However, in the absence of multi-path, the received samples have structure (19), and the transmitted sequences can be designed, so that the complexity of detection at the receiver can be reduced.

The key strategy for reducing the detection complexity is to exploit orthogonality among sub-sequences of transmitted symbols. Offset-quadrature PSK modulation (9) alternates one-dimensional modulation symbols along the in-phase and quadrature components, which allows the optimum symbol-by-symbol decisions.

Multiplexing two data streams as described by (23) can exploit the design principles of superposition modulation and multiuser detection. In such a case, symbol-by-symbol decisions can be performed by SIC. Specifically, provided that symbols,  $b_n$ , can be reliably detected, even if the symbols,  $(a_n + a_{n+1})/2$ , are not yet known, then the symbol,  $a_n$ , can be reliably detected after canceling the ISI term,  $(b_{n-1} + b_n)/2$ .

In the sequel, three other sequence design strategies are discussed in more detail. The first strategy combines pilot and data symbols to aid the data detection and channel estimation. The second strategy employs orthogonal spreading codes in order to separate the two multiplexed data sequences. The third strategy adopts the differential encoding of transmitted symbols.

### B. Sequences with Interleaved Pilot Symbols

In general, pilot symbols for channel estimation can be interleaved with data symbols or superimposed onto data symbols [17]. Here, the more common former approach is adopted. Thus, consider a transmitted sequence consisting of alternating groups of  $L_d$  data symbols and  $L_p \ll L_d$  pilot symbols, which are separated by a single zero-symbol as shown in Fig. 4.

For instance, the following sub-sequences with reduced or no ISI can be considered with pilot symbol,  $p$ , and arbitrary data symbols,  $d_1$ , and,  $d_2$ :  $(0, p, 0)$ ,  $(d_1, p, -d_1)$ ,  $(d_1, p, -d_1, -p, d_1)$ , and  $(d_1, p, -d_1, -p, d_2, p, -d_2)$ . These sub-sequences enable ISI-free data detection and channel estimation, as can be deduced from eq. (23) and Fig. 3. Recall also that the noise samples,  $w_n$ , and,  $w_{n\pm 2}$ , are uncorrelated, i.e., independent.

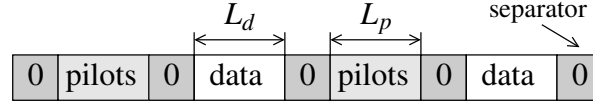


Fig. 4. The transmitted sequence with interleaved sub-sequences of data and pilot symbols and a single zero-symbol separator.

In order to illustrate the ISI-free channel estimation, consider the sequence,  $(d_1, p, p, -d_1)$ . The received samples corresponding to the two pilot symbols in the middle are,

$$\begin{aligned} r_n &= h \frac{3}{2} p + h \frac{1}{2} d_1 + w_n \\ r_{n+1} &= h \frac{3}{2} p - h \frac{1}{2} d_1 + w_{n+1} \end{aligned} \quad (26)$$

where  $h$  denotes the complex-valued channel attenuation (i.e., frequency non-selective slow fading). The samples,  $r_n$ , and,  $r_{n+1}$ , can be simply combined as,

$$r_n + r_{n+1} = 3hp + w_n + w_{n+1} \quad (27)$$

where the total variance of the additive noise samples is equal to  $3\sigma_w^2$  due to correlations (20).

More generally, the transmitted sequence,

$$(-p, d_1, p, d_2, -p, d_3, p, d_4, -p, d_5, \dots, d_N, \pm p) \quad (28)$$

where the last pilot symbol is  $p$ , if  $N$  is odd, and  $-p$ , if  $N$  is even, allows the ISI-free symbol-by-symbol decisions of all data symbols. Moreover, assuming again a slow fading channel, the received samples corresponding to the pilot symbols can be summed up to obtain,

$$\sum_{n=1}^N (-1)^n r_{2n-1} = N h p + \sqrt{N} w$$

where the noise sample,  $w$ , has the variance,  $\sigma_w^2$ , so the signal-to-noise ratio (SNR) for estimating the channel coefficient,  $h$ , has been improved  $N$ -times. Note also that once the channel has been estimated, the pilot symbols can be subtracted from the received samples in order to aid decisions of the remaining data symbols.

Finally, consider the case of a symbol repetition diversity. The transmitted sequence,  $(d, 0, d, 0, \dots, 0, d)$ , of a data symbol,  $d$ , repeated  $(N \geq 2)$ -times corresponds to the canonical Nyquist signaling. The pulse-shape multiplex modulation instead transmits the sequence,  $(d, d, \dots, d)$ , of  $N_1$ -times repeated data symbol,  $d$ . For the same sequence length,  $N_1 = 2N - 1$ . Assuming slowly

fading channel, the detector combines the received samples for the two modulation schemes, respectively, as,

$$\begin{aligned} r &= N h d + \sqrt{N} w \\ r &= (2 \cdot 3/2 + 2(N_1 - 2)) h d / \sqrt{2} + \sqrt{2N_1 - 1} w \end{aligned} \quad (29)$$

where the scaling by  $\sqrt{2}$  was introduced for the second modulation in order to account for the larger number of symbols in its transmitted sequence. The resulting SNR of these two schemes is proportional to,  $\gamma \propto N$ , and,  $\gamma \propto 2N - 3/2$ , respectively. Consequently, for symbol repetition diversity, the SNR gain of the pulse-shape binary multiplexing is asymptotically 3 dB larger than for the Nyquist signaling.

### C. Sequences with Orthogonal Spreading

Another strategy for transmitting interleaved, but orthogonal symbols in modulated signal (18) is to use orthogonal spreading codes. In particular, assume transmitted symbols,

$$a_n = d_1 c_n^{(1)}, \quad b_n = d_2 c_n^{(2)} \quad (30)$$

where  $d_1$  and  $d_2$  are two data symbols, and,  $c_n^{(1)}$  and  $c_n^{(2)}$ ,  $n = 1, 2, \dots, N$ , are generally complex-valued, orthogonal spreading sequences, so that,

$$\sum_{n=1}^N c_n^{(i)} c_n^{*(j)} = \begin{cases} N, & i = j \\ 0, & i \neq j. \end{cases} \quad (31)$$

Then, the sequences of received samples (23) are linearly combined as,

$$\begin{aligned} \sum_{n=1}^N r_{2n-1} c_n^{*(1)} &= d_1 + d_2 \sum_{n=1}^N \frac{c_n^{(2)} + c_{n+1}^{(2)}}{2} c_n^{*(1)} + \sum_{n=1}^N w_{2n-1} c_n^{*(1)} \\ &= d_1 + \tilde{w}_1 \\ \sum_{n=1}^N r_{2n} c_n^{*(2)} &= d_2 + d_1 \sum_{n=1}^N \frac{c_n^{(1)} + c_{n+1}^{(1)}}{2} c_n^{*(2)} + \sum_{n=1}^N w_{2n} c_n^{*(2)} \\ &= d_2 + \tilde{w}_2 \end{aligned} \quad (32)$$

provided that the spreading sequences,  $c_n^{(1)}$ , and,  $c_n^{(2)}$ , are exactly orthogonal. In such a case, the SNR improvement for transmitting two data symbols with orthogonal spreading sequences using the pulse-shape binary multiplex modulation (18) is proportional to,

$$\gamma \propto \frac{N^2}{2N - 1}. \quad (33)$$

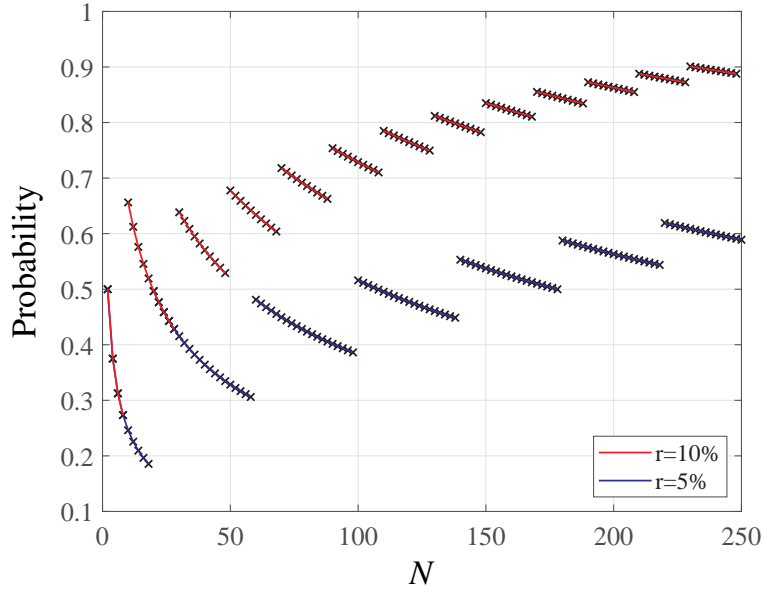


Fig. 5. The probability (35) vs. the spreading sequence length,  $N$ , assuming  $\kappa = 5\%$  and  $\kappa = 10\%$ , respectively.

For instance, if the spreading symbols,  $c_n$ , are generated independently at random and with an equal probability from the set,  $\{-1, +1\}$ , the probability that two such sequences are orthogonal is,

$$\begin{aligned} \Pr\left(\sum_{n=1}^N c_n^{(1)} c_n^{*(2)} = 0\right) &= \binom{N}{N/2} \left(\frac{1}{2}\right)^{N/2} \left(\frac{1}{2}\right)^{N-N/2} \\ &= \binom{N}{N/2} 2^{-N}. \end{aligned} \quad (34)$$

Since the probability (34) of exact orthogonality asymptotically goes to zero with large  $N$ , consider instead the probability,

$$\begin{aligned} \Pr\left(-\lceil \kappa N/2 \rceil \leq \sum_{n=1}^N c_n^{(1)} c_n^{*(2)} \leq \lceil \kappa N/2 \rceil\right) \\ = \sum_{n=-\lceil \kappa N/2 \rceil}^{\lceil \kappa N/2 \rceil} \binom{N}{n} \left(\frac{1}{2}\right)^N \end{aligned} \quad (35)$$

for some small  $\kappa \geq 0$ . The probabilities (35) as a function of  $N$  for two different values of factor,  $\kappa$ , are shown in Fig. 5. These probabilities are indicative of how many random spreading sequences need to be generated in order to select the required number of such sequences having an acceptable level of mutual orthogonality.

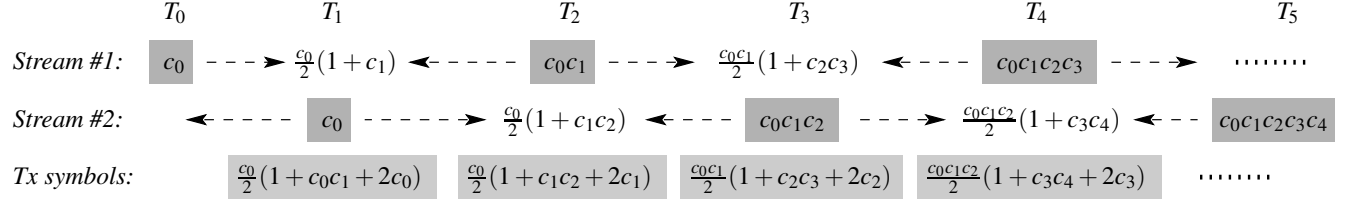


Fig. 6. Differentially encoded  $M$ -ary PSK symbols transmitted via pulse-shape binary multiplex modulation.

#### D. Sequences with Differential Encoding

Differential PSK is a popular modulation scheme for fast fading channels, since it alleviates the need for recovering the absolute phase reference. Fig. 6 shows differentially encoded  $M$ -ary PSK symbols (8) transmitted via pulse-shape binary multiplex modulation. In particular, the  $n$ -th transmitted symbol is,

$$\begin{aligned}
 s_n &= \left( \prod_{k=0}^{n-2} c_k \right) \frac{1 + c_{n-1}c_n + 2c_{n-1}}{2} \\
 &= \frac{1}{2} \left( \prod_{k=0}^{n-2} c_k \right) + \frac{1}{2} \left( \prod_{k=0}^{n-1} c_k \right) c_n + \left( \prod_{k=0}^{n-1} c_k \right).
 \end{aligned} \tag{36}$$

Consequently, the differential decoding can be performed as,

$$\begin{aligned}
 c_n &= \left( 2s_n - \left( \prod_{k=0}^{n-2} c_k \right) - 2 \left( \prod_{k=0}^{n-1} c_k \right) \right) \left( \prod_{k=0}^{n-1} c_k \right)^* \\
 &= 2s_n \left( \prod_{k=0}^{n-1} c_k^* \right) - c_{n-1}^* - 2.
 \end{aligned} \tag{37}$$

The performance of this modulation scheme is evaluated in the next section.

#### V. NUMERICAL EXAMPLES

It is convenient to use a vector notation to generate samples of pulse-shape binary multiplex modulation (18) received over a frequency non-selective fading channel. The vector,  $\mathbf{r}$ , of  $N$  received samples corresponding to the vector,  $\mathbf{s}$ , of  $N$  transmitted symbols can be obtained as,

$$\mathbf{r} = \mathbf{s} \mathbf{A} \text{diag}(\mathbf{h}) + \mathbf{w} \mathbf{A}_0^T$$

where  $\mathbf{h}$  is a vector of fading channel coefficients,  $\mathbf{w}$  are samples of AWGN, and the  $(N \times N)$  ISI matrix,

$$\mathbf{A} = \begin{bmatrix} 1 & 1/2 & & \\ 1/2 & 1 & 1/2 & \\ & \ddots & \ddots & \\ & & 1/2 & 1 \end{bmatrix} = \mathbf{A}_0 \mathbf{A}_0^T.$$

The optimum detection requires that the additive noise is first whitened as, [4]

$$\mathbf{r} \mathbf{A}_0^{-T} = \mathbf{s} \mathbf{A} \text{diag}(\mathbf{h}) \mathbf{A}_0^{-T} + \mathbf{w}.$$

Then the maximum likelihood (ML) detection of sequence  $\mathbf{s}$  is,

$$\hat{\mathbf{s}} = \arg \min_{\mathbf{s}} \left\| \mathbf{r} \mathbf{A}_0^{-T} - \mathbf{s} \mathbf{A} \text{diag}(\hat{\mathbf{h}}) \mathbf{A}_0^{-T} \right\|^2 \quad (38)$$

where  $\hat{\mathbf{h}}$  is the estimate of  $\mathbf{h}$  representing channel state information (CSI).

An uncoded binary phase shift keying (BPSK) modulation and Rayleigh-distributed fading amplitudes,  $\mathbf{h}$ , are assumed for simplicity. The transmitted sequence interleaves pilot symbols and data symbols as shown in Fig. 4. The pilot symbols are used to estimate the channel coefficients,  $\mathbf{h}$ , by linear minimum mean-square error (LMMSE) algorithm. The spectral efficiency of pulse-shape binary multiplexing is, 2, which is always larger than the spectral efficiency of the Nyquist signaling being equal to,  $2/(1 + \alpha)$ .

The BER curves,  $P_e$ , for short data sequences of  $L_d = 4$  and  $L_d = 8$  binary symbols, respectively, separated by a single zero-symbol are shown in Fig. 7 and Fig. 8. The SNR is defined as,  $\gamma_b = 1/(2\sigma_w^2)$ . Both cases of perfect and estimated CSI are considered. The Nyquist signaling (no ISI) with symbol-by-symbol decisions is assumed as a reference. The ML data detector (38) is used for pulse-shape multiplexing signaling.

It can be observed that the performance penalty due to channel estimation is much larger for pulse-shape multiplexing than for the Nyquist signaling, which is to be expected. The WMF improves the performance by several dB's for both signaling schemes. More importantly, the performance of pulse-shape multiplexing improves with the data block length by exploiting the time diversity over a fading channel, so it can significantly outperform the Nyquist signaling at medium to large SNR values. It is likely that by employing more sophisticated channel estimation and equalization techniques, the performance of pulse-shape multiplexing can be further improved. In order to demonstrate the effect of time diversity, Fig. 9 shows that, over



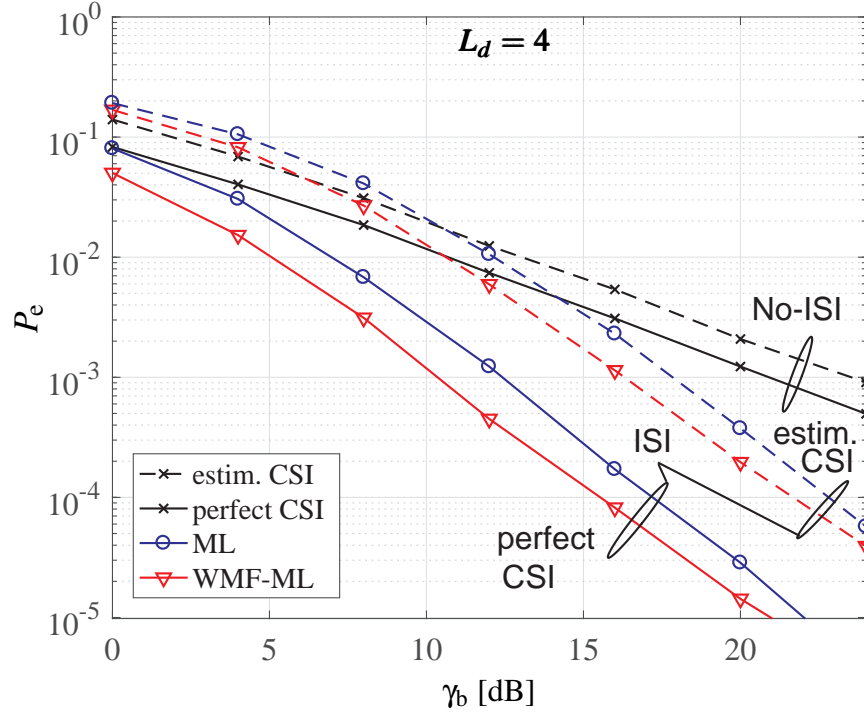


Fig. 7. The BER of BPSK vs. SNR over Rayleigh fading channel for sequences of 4 binary symbols.

an AWGN channel, the performance of pulse-shape multiplexing is worse than that of Nyquist signaling, even though some performance loss can be recovered by WMF.

Lastly, the BER performance of Nyquist modulation and pulse-shape multiplex modulation transmitting differentially encoded quadrature PSK (QPSK) symbols over an AWGN channel is compared in Fig. 10. It can be observed that even though the pulse-shape multiplexing suffers asymptotically a 3 dB penalty in SNR, it reduces the time required for transmitting the whole symbol sequence to one half.

## VI. CONCLUSION

The paper introduced a pulse-shape binary multiplex modulation. Such a modulation scheme is akin to partial-response signaling, correlative coding, offset-QPSK modulation and FTN signaling. It combines two data streams under controlled ISI created by the RRC pulses having 100% roll-off, and transmitted at twice the Nyquist rate. The ISI analysis showed that this is unique property among all the roll-off factors being at most 100% and the packing factors greater than 5%. However, the successive samples of additive noises at the output of matched filter at

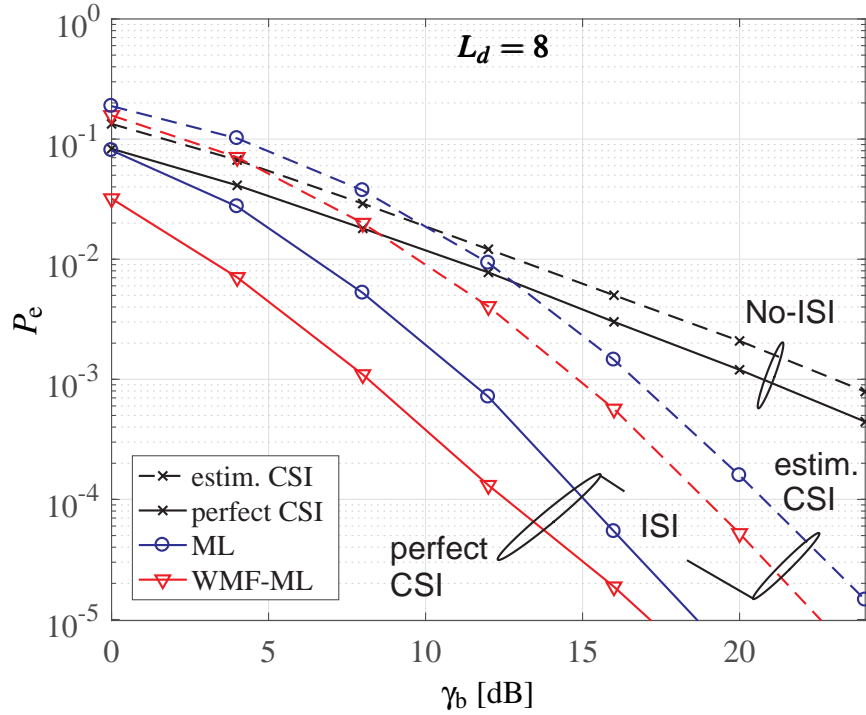


Fig. 8. The BER of BPSK vs. SNR over Rayleigh fading channel for sequences of 8 binary symbols.

the receiver become correlated, which incurs a SNR performance penalty. This penalty could be reduced or even removed by using more complex sequence-based detection schemes as shown elsewhere in the literature. The BER performance as well as decoding complexity of the proposed pulse-shape binary multiplexing modulation scheme is critically affected by the choice of transmitted sequences. One can consider superposition modulation with SIC decoding, interleave data symbols with pilot and zero-symbols to aid channel estimation and data decoding, and also employ orthogonal spreading sequences to separate the multiplexed data streams. The numerical results indicate that pulse-shape binary multiplexing can exploit time-diversity in fading channels to outperform the Nyquist signaling. In addition, it has been shown numerically that a sequence of differentially encoded PSK symbols can be transmitted twice as fast by the proposed modulation scheme compared to canonical Nyquist signaling, although with a 3 dB SNR penalty over AWGN channels.

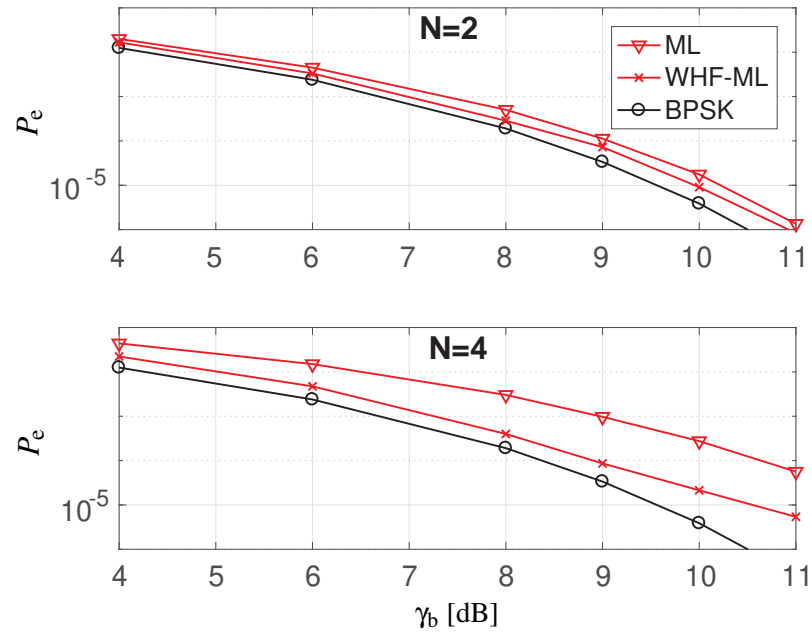


Fig. 9. The BER of BPSK vs. SNR over AWGN channel for sequences of 2 and 4 binary symbols, respectively.

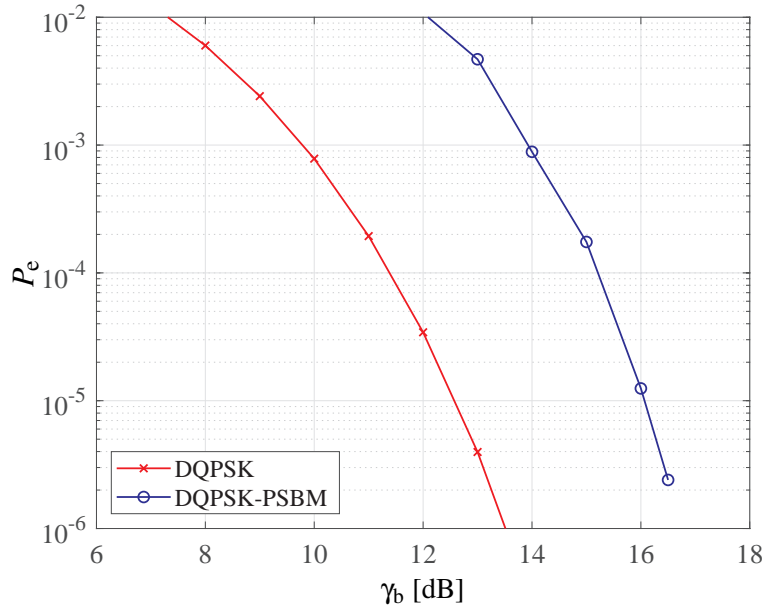


Fig. 10. The BER comparison of differentially encoded QPSK with Nyquist and pulse-shape binary multiplexing (PSBM) modulation transmitted over an AWGN channel.

## REFERENCES

- [1] J. Zhou, D. Li, and X. Wang, "Generalized Faster-Than-Nyquist signaling," in *ISIT*, 2012, pp. 1478–1482.
- [2] J. B. Anderson, F. Rusek, and V. Öwall, "Faster-Than-Nyquist signaling," *Proc. of the IEEE*, vol. 101, no. 8, pp. 1817–1830, August 2013.
- [3] A. Liveris and C. Georgiades, "Exploiting Faster-Than-Nyquist signaling," *IEEE Transactions Communications*, vol. 51, no. 9, pp. 1502–1511, September 2003.
- [4] J. G. Proakis and M. Salehi, *Digital Communications*, 5th ed. McGraw-Hill Education, NY, USA, 2008.
- [5] L. Landau, M. Dörpinghaus, and G. P. Fettweis, "1-bit quantization and oversampling at receiver: Communication over bandlimited channels with noise," *IEEE Comm. Letters*, vol. 21, no. 5, pp. 1007–1010, May 2017.
- [6] A. Modenini, G. Colavolpe, and N. Alagha, "How to significantly improve the spectral efficiency of linear modulations through time-frequency packing and advanced processing," in *Proc. ICC*, 2012, pp. 3260–3264.
- [7] J. Fan, S. Guo, X. Zhou, Y. Ren, G. Y. Li, and X. Chen, "Faster-Than-Nyquist signaling: An overview," *IEEE Access*, vol. 5, pp. 1925–1940, February 2017.
- [8] Y. Yamada, M. Sawahashi, and K. Saito, "Performance of time and frequency compression of Faster-than-Nyquist signaling in frequency-selective fading channels," in *APCC*, 2015, pp. 550–554.
- [9] T. E. Bogale, L. B. Le, X. Wang, and L. Vandendorpe, "Multipath multiplexing for capacity enhancement in SIMO wireless systems," *IEEE Transactions Wireless Communications*, vol. 16, no. 10, pp. 6895–6911, October 2017.
- [10] H. Zhang, X. Huang, J. A. Zhang, and Y. J. Guo, "Dual pulse shaping transmission and equalization for high-speed wideband wireless communication systems," *IEEE Transactions on Circuits and Systems I*, vol. 67, no. 7, pp. 1549–8328, July 2020.
- [11] H. Li, X. Huang, J. A. Zhang, H. Zhang, and Z. Cheng, "Dual pulse shaping transmission with sinc-function based complementary Nyquist pulses," *IET Communications*, vol. 16, no. 17, pp. 2091–2104, October 2022.
- [12] E. Bedeer, M. H. Ahmed, and H. Yanikomeroglu, "A very low complexity successive symbol-by-symbol sequence estimator for Faster-Than-Nyquist signaling," *IEEE Access*, vol. 5, pp. 7414–7422, June 2017.
- [13] J. Bas and A. A. Dowhuszko, "Linear time-packing detectors for optical feeder link in high throughput satellite systems," in *GC-ElecEng*, 2020, pp. 21–26.
- [14] Q. Shi, N. Wu, X. Ma, and H. Wang, "Frequency-domain joint channel estimation and decoding for Faster-Than-Nyquist signaling," *IEEE Transactions Communications*, vol. 66, no. 2, pp. 781–795, February 2018.
- [15] N. Wu, W. Yuan, Q. Guo, and J. Kuang, "A hybrid BP-EP-VMP approach to joint channel estimation and decoding for FTN signaling over frequency selective fading channels," *IEEE Access*, vol. 5, pp. 6849–6858, May 2017.
- [16] P. Loskot, "A generalized FSK-based PHY layer design for wireless sensor networks," in *Chinacom*, 2012, pp. 362–367.
- [17] A. K. Jagannatham and B. D. Rao, "Superimposed pilots vs. conventional pilots for channel estimation," in *ACSSC*, 2006, pp. 767–771.